Journal of Chromatography A, 1218 (2011) 4138–4143

Contents lists available at ScienceDirect

Journal of Chromatography A

journal homepage: www.elsevier.com/locate/chroma

Inertial separation in a contraction–expansion array microchannel

Myung Gwon Lee[a,1], Sungyoung Choi[a,1,2], Je-Kyun Park[a,b,*]

[a] Department of Bio and Brain Engineering, College of Life Science and Bioengineering, Korea Advanced Institute of Science and Technology (KAIST), 291 Daehak-ro, Yuseong-gu, Daejeon 305-701, Republic of Korea
[b] KAIST Institute for the NanoCentury, 291 Daehak-ro, Yuseong-gu, Daejeon 305-701, Republic of Korea

ARTICLE INFO

Article history:
Available online 5 December 2010

Keywords:
Microfluidics
Inertial separation
Contraction–expansion array microchannel
Dean flow
Fluorescent solution

ABSTRACT

We report a contraction–expansion array (CEA) microchannel that allows inertial size separation by a force balance between inertial lift and Dean drag forces in fluid regimes in which inertial fluid effects become significant. An abrupt change of the cross-sectional area of the channel curves fluid streams and produces a similar effect compared to Dean flows in a curved microchannel of constant cross-section, thereby inducing Dean drag forces acting on particles. In addition, the particles are influenced by inertial lift forces throughout the contraction regions. These two forces act in opposite directions each other throughout the CEA microchannel, and their force balancing determines whether the particles cross the channel, following Dean flows. Here we describe the physics and design of the CEA microfluidic device, and demonstrate complete separation of microparticles (polystyrene beads of 4 and 10 μm in diameter) and efficient exchange of the carrier medium while retaining 10 μm beads.

1. Introduction

Separation and filtration of particles are important for a wide range of applications in a biochemical, clinical, and environmental field [1–3]. Recent advances in microfluidics have been brought about a great number of separation methods, such as magnetophoresis [4], dielectrophoresis [5,6], and optical [7] and acoustic [8] separations. However, these techniques require external forces applied to particles in a continuous flow, resulting in various limitations, including low-throughput due to the decreasing time for the forces acting on particles with increasing flow rate and difficulties of integration of active sources.

A few of passive and continuous separation methods using inertial fluid behaviors in microfluidic devices have recently been reported to overcome these limitations. The inertial fluid induces inertial hydrodynamic forces (*i.e.*, wall-induced inertial lift forces, shear-induced inertial lift forces and Dean drag forces) along with increase of flow rate, enabling particle separation with high throughput and without external forces. In a cylindrical tube, particles were observed to migrate away from the tube center and walls due to the inertial fluids. This is known as the "tubular pinch effect" [9–11]. This inertial migration phenomenon can be explained by combination of wall-induced inertial lift force and shear-induced inertial lift force. Inertial migration by the inertial lift forces has been investigated by numerical simulation at a wide range of Reynolds number (Re) up to 1000. The migrated particles in a square duct were located at eight and four equilibrium positions corresponding to Re of 100 and 500, respectively [12]. In order to equilibrate the particles at low flow rates (Re < 50), the large inertial lift forces were generated by high shear rate in rectangular microchannels with high aspect ratios, which achieved a reduction from multi equilibrium positions to two equilibrium positions of the particles [13]. In spite of focusing particles to certain positions using the inertial lift forces, it is required to focus particles in a single position for completely separating particles from the other particles and solutions. Di Carlo et al. [14] reduced the deviation of the particle equilibrium position in an asymmetric curvilinear microchannel using Dean drag forces from Dean flows which arises at a curvature region of the channel. From the experimental data and theoretical calculations, they observed that particles can be focused in a single equilibrium position with $a_p/D_h > 0.07$ (a_p: particle diameter, D_h: hydraulic diameter) and lose it below that value. However, the asymmetric curvilinear design is substantially complicated to easily understand how the inertial lift and Dean drag forces play role in focusing particles; and then to modify its design for proper microfluidic separation.

On the other hand, centrifugal forces were for the first time considered in spiral microchannels with high aspect ratios and demonstrated the separation of 1, 8, and 10 μm polystyrene parti-

* Corresponding author at: Department of Bio and Brain Engineering, College of Life Science and Bioengineering, Korea Advanced Institute of Science and Technology (KAIST), 291 Daehak-ro, Yuseong-gu, Daejeon 305-701, Republic of Korea. Tel.: +82 42 350 4315; fax: +82 42 350 4310.
E-mail address: jekyun@kaist.ac.kr (J.-K. Park).
[1] These authors contributed equally to this work.
[2] Current address: Department of Mechanical Engineering, Massachusetts Institute of Technology, Cambridge, MA 02139, USA.

0021-9673/$ – see front matter © 2010 Elsevier B.V. All rights reserved.
doi:10.1016/j.chroma.2010.11.081

cles [15]. The spiral microchannel design was slightly modified with the "S" shaped-center junction added for reversing the direction of flow, and separation of particles less than 10 μm in diameter was tested in the design, resulting in effective focusing of the 10 μm particles [16]. Even though the separation principle in the spiral design was illustrated with combined inertial effects, including centrifugal force, lift force, lateral force, and Dean vortex flow, it was not sufficient to understand the mechanism of the particle separation. From numerical and experimental results, the separation mechanism in the spiral design was described in detail how the particles theoretically migrate under the influence of interaction between the inertial lift and Dean drag forces, and complete separation of two different-sized particles (1.9 and 7.32 μm) were demonstrated in the spiral microchannel [17]. However, the spiral design does not constantly sustain the Dean drag forces being a function of radius of curvature due to the geometrical changes of curvature along the channel, and it also requires long distance of the channel for separation with inertial fluids.

To overcome the above limitations, we utilize a contraction–expansion array (CEA) microchannel design where inertial effects such as inertial lift and Dean drag forces are constrained to occur in fixed directions and magnitudes. The design of CEA microchannel has been described in our previous publications [18–20], in which we have investigated an inertial fluid behavior and the Dean flow in the CEA microchannel that constrain the Dean flow to arise in fixed directions without flow reversal problem. These phenomena have been used for three-dimensional hydrodynamic focusing and mixing. In those applications, the inertial lift forces are negligible. The small particles such as red blood cells and fluorescein are dominantly influenced by Dean flow rather than the inertial lift forces. In this paper, however, we consider both forces for inertial size separation and investigate the effect of the force balance between these forces. Using this approach, we demonstrate complete separation of microparticles (polystyrene beads of 4 and 10 μm in diameter) and efficient exchange of the carrier medium while retaining 10 μm beads.

2. Experimental

2.1. Channel design and fabrication

Fig. 1a shows the micrograph of the CEA microchannel. The CEA microchannel was 350 μm wide and 38 μm deep, with contraction regions of 50 μm wide and 300 μm long. The interval between contraction regions was 300 μm. An observation window was located after every sixth rectangular structures in the microchannel and the CEA microchannel was composed of thirty rectangular structures. The CEA microchannel was fabricated in poly(dimethylsiloxane) (PDMS) using soft lithography techniques. A mixture of PDMS prepolymer and its curing agent (Sylgard 184; Dow Corning, MI) in the ratio of 9:1 was poured on the SU-8 photoresist molds and cured for 3 h in a convection oven at 65 °C. Irreversible bonding was made between a PDMS replica and a glass slide, treating both of them with oxygen plasma (200 mTorr, 200 W).

2.2. Computational fluid dynamic simulation

Computational fluid dynamics (CFD) simulation for flow characteristics of the CEA microchannel was performed using a commercial CFD solver (CFD-ACE+; ESI Group, Huntsville, AL). The physical properties of water were applied to the fluids traveling through the CEA microchannel (density $\rho = 997\ kg/m^3$ and dynamic viscosity $\mu = 8.55 \times 10^{-4}\ kg/ms$). The applied total flow rates (the sum of the flow rates of the injected sample and focusing flow) were varied from 3 to 22 mL/h, while the outlet was set to a

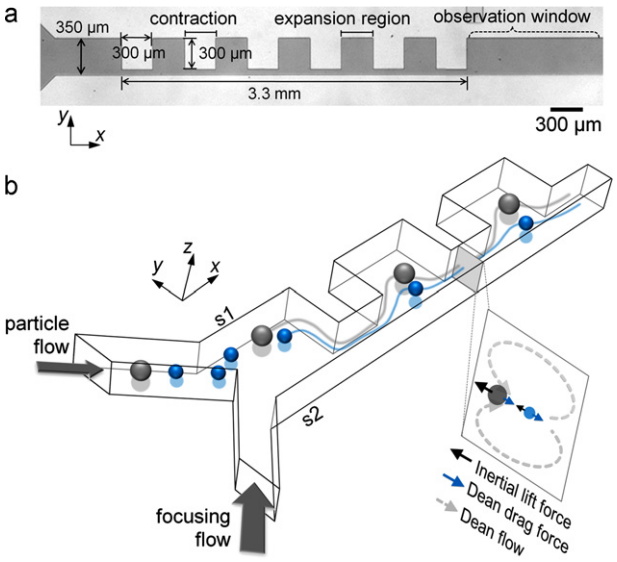

Fig. 1. Contraction–expansion array (CEA) microchannel. (a) Micrograph of the fabricated CEA microchannel. Each rectangular structure was formed for contraction and expansion regions in the microchannel. An observation window was used to measure inertial separation of particles after every sixth rectangular structure. (b) Schematic of the proposed CEA microchannel for inertial size separation. Neutrally buoyant particles flow along sidewall 1 of the channel by a focusing flow and experience both inertial lift and Dean drag forces. The direction of particle migration is determined by balancing the magnitudes of two forces. At a proper flow condition, the different-sized particles can have an opposite direction of migration, resulting in separating each other: the large particles to sidewall 1 and the smaller particles to sidewall 2 (s1: sidewall 1, s2: sidewall 2).

fixed-pressure boundary condition. The algebraic multigrid (AMG) solver was used for pressure correction, and the conjugates gradient squared (CGS) solvers were used for velocity of the flow. The convergence limit and iteration were set to 10^{-4} and 10^4 time steps until the flow reached the outlet.

2.3. Experimental setup

Red fluorescent polystyrene beads of 4 and 15 μm in diameter; and green fluorescent polystyrene bead of 10 μm in diameter (Molecular Probes, Eugene, OR) were used for inertial separation. All beads were prepared in 0.2% Pluronic solution (Sigma–Aldrich Co., St. Louis, MO) with a concentration of 8.5×10^5, 3.3×10^5 and 6.3×10^4 particles/mL, respectively. We used the 0.2% Pluronic solution to minimize polystyrene-bead sticking to the channel wall and other polystyrene beads. Fluorescein (Sigma–Aldrich Co.) solution with a concentration of 50 μg/mL was also used for exchange of the carrier medium. A fluorescent fluid containing microparticles; and non-fluorescent focusing fluid (0.2% Pluronic solution) were injected into the CEA microchannel using syringe pumps (KDS200; KD Scientific Inc., Holliston, MA) at specified total flow rates from 3 to 22 mL/h, constantly sustaining the flow ratio between the particles and focusing flow as 1:5. The trajectories of the particles were visualized using a fluorescence microscope (TS100; Nikon Co., Japan) equipped with a charge-coupled device (DS-2MBWc; Nikon Co.) with a long exposure time of 1 s or less. The collected solutions after medium exchange were measured for emission wavelength of fluorescein using a spectrometer (MicroSpec 2300i; Princeton Instruments, Trenton, NJ) equipped with a charge-coupled device (PIXIS 400B; Princeton Instruments).

2.4. Measurement

The acquired images with the fluorescence microscope were processed with ImageJ software (http://rsb.info.nih.gov/ij/). The

mean lateral position (Y_{Mean}) of the particles was calculated according to the following formulation:

$$Y_{Mean} = \frac{\sum_{i=1}^{n} y_i I_i}{\sum_{i=1}^{n} I_i} \quad (1)$$

where y_i refers to pixels (between 0 and 1) measured relative to the lateral position in the contraction region, and I_i refers to the grayscale values of each pixel. The calculated values of each pixel are converted for representing the lateral position of the channel. The separation resolution, R_s, between two different-sized particles is defined as $R_s = 0.5(\Delta Y/(\sigma_1 + \sigma_2))$, where ΔY is the distance between mean lateral position of two particles and σ is the standard deviation of lateral position of each particle [21].

3. Results and discussion

3.1. Design principle

Fig. 1b shows the schematic of the proposed CEA microchannel for inertial size separation. In order to separate particles by inertial effects: (1) inertial lift migration and (2) Dean flow, we designed an array of contraction and expansion region in the microchannel. To achieve the complete inertial separation of the particles, the direction of rotation of the Dean flow is necessary to be sustained throughout the CEA microchannel, thereby continuously balancing with inertial lift forces. In consideration of the above matter, we designed the one-sided rectangular structures to induce the Dean flow sustaining in the fixed direction. This proposed channel design utilizes an abrupt change of the cross-sectional area of the channel that curves fluid streams, and accelerates or decelerates the flow velocity along the contraction and expansion region, respectively. When the fluid enters into the contraction region, the streamlines from the wider part of the upstream microchannel accelerate and follow a curved path, producing Dean flows. In contrast, the fluid entering the expansion region decelerates due to the increase of cross-sectional area and any Dean-like flow effects are offset by the deceleration. Therefore, centrifugal effects are dominant at the entrance of the contraction regions, resulting in a secondary, transverse flow field characterized by two counter rotating vortices in the upper and lower plane of symmetry of the channel.

The parabolic nature of a velocity profile in a rectangular microchannel results in shear-induced inertial lift forces that enable particles to migrate away from the channel center toward the sidewalls. When the particles are close to the sidewall, an asymmetric wake around the particles generates wall-induced inertial lift forces that drive the particles away from the channel wall to the channel center [14]. By balancing between the two different inertial lift forces, the particles thus occupy two equilibrium positions predicted at $\approx 0.2D_h$ away from the sidewalls [10,11,22,23]. These inertial lift forces are caused throughout the CEA microchannel, especially in the contraction region due to high shear rate. The rectangular cross-section of the contraction regions in the CEA microchannel yields a higher shear rate between the sidewalls than that of the expansion regions, which results in large lift forces that drive the particles toward the equilibrium positions more quickly. The large lift forces in the contraction regions thus reduce the required channel length for complete migration of the particles across streamlines to occupy their equilibrium position [13].

When the particles flow along sidewall 1 of the channel by a focusing flow in the CEA microchannel, various forces act on the particles, such as shear-induced, wall-induced lift forces, and Dean drag forces. Without the influence of Dean drag forces, the particles can occupy an equilibrium position predicted at $\approx 0.2D_h$ away from sidewall 1. Under the influence of Dean drag forces, a new equilibrium position is formed at the position of $>0.2D_h$ from sidewall 1 by balancing with the inertial lift forces. Consequently, the particles flowing along sidewall 1 experience inertial lift forces that move particles away from the channel center and Dean drag forces by the Dean flow directing from sidewall 1 to sidewall 2. Magnitudes and directions of the migration of the particles across streamlines are determined depending on the magnitude of these forces. When the magnitude of the inertial lift forces is larger than that of the Dean drag forces, the particles migrate toward sidewall 1 and occupy their equilibrium position where the sum of these forces becomes zero. In an opposite magnitude of these forces, the particles migrate toward sidewall 2, following the Dean flows.

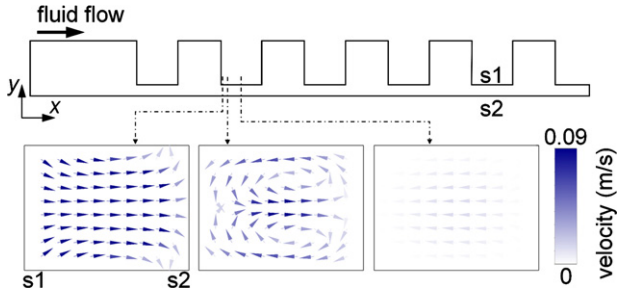

Fig. 2. Simulation results of transverse velocity (y-velocity) vector fields representing Dean flows at the cross-sections of the second contraction region. The cross-sectional images obtained at x-axial position of 5, 35 and 150 μm apart from the beginning of the second contraction regions at a total flow rate of 6 mL/h.

3.2. Theoretical analysis by numerical simulation results

To verify Dean flows in the contraction region, computational numerical simulation was performed with flowing fluids in the CEA microchannel. From the numerical simulation results, two counter-rotating Dean vortices causing transverse velocity fields appear to be completely developed around the x-axial position of 35 μm apart from the beginning of the contraction region (Fig. 2). In the transverse velocity field, the Dean drag forces (F_D) acting on the particles can be obtained by assuming the Stokes drag:

$$F_D = 3\pi\mu U_{Dean} a_p \quad (2)$$

where μ, U_{Dean} and a_p are the density of the fluids, transverse velocity by Dean flow and particle diameter, respectively.

The inertial lift forces also act on the particles flowing through the contraction region. The level of forces highly depends on particle size. Inertial lift forces are dominant on the particles when the particle Reynolds number (Re_p) is of order 1. The particle Reynolds number is defined as,

$$Re_p = Re_c \frac{a_p^2}{D_h^2} = \frac{\rho U_m a_p^2}{\mu D_h} \quad (3)$$

where Re_c, D_h, ρ and U_m are the channel Reynolds number, the hydraulic diameter defined as $2wh/(w+h)$ (w: width of contraction channel, h: height of the channel), the density of the fluid and maximum flow velocity, respectively. In the case of $Re_p \ll 1$, particle flow in the microchannel is dominated by viscous drag force acting on the particle surface [14]. The inertial lift forces drive the particles away from the channel center to an equilibrium position. Asmolov [24] derived an expression for the inertial lift force (F_L) acting on the particles, assuming $Re_p < 1$:

$$F_L = \frac{\rho U_m^2 a_p^4 C_L}{D_h^2} \quad (4)$$

where ρ is the density of the fluid and C_L is the lift coefficient which is a function of the particle position across the channel. The lift coefficient is zero at the channel center and equilibrium position

[24,25]. Because the particles occupy an equilibrium position in the CEA microchannel at the same magnitude of inertial lift force and Dean drag force, we can obtain the lift coefficient using above expressions of F_D and F_L at the equilibrium position. In this theoretical analysis, we assumed that these inertial effects work only in the contraction region ($Re_p \approx 1$, for 10-μm sized particles at 3 mL/h) because an influence of inertial lift and Dean drag forces acting on particle may barely exist in the expansion regions ($Re_p \approx 0.09$). In the contraction regions, we observed that the mean equilibrium position of 10-μm sized particles is formed at ≈36 μm from sidewall 2 from the experimental results. Thereafter, we obtained values of U_{Dean} and U_m by means of the computational numerical simulation at the equilibrium position, position of 36 μm from sidewall 2 and middle of the channel height along the contraction regions. From the obtained values, we can calculate F_D and F_L at the equilibrium position and finally acquire the lift coefficient of ≈0.09. Using the acquired lift coefficient, the Dean drag force (F_D) and inertial lift force (F_L) acting on 4 and 10 μm particles are obtained. At a total flow rate of 3 mL/h, F_L and F_D are 0.118 μN and 0.118 μN for 10 μm particles; and 0.003 μN and 0.047 μN for 4 μm particles, respectively. From these calculations, we can expect that the 10 μm particles occupy the equilibrium position while the 4 μm particles move toward sidewall 2. At a total flow rate of 6 mL/h, F_L and F_D are 0.454 μN and 0.413 μN for 10 μm particles; and 0.012 μN and 0.165 μN for 4 μm particles, respectively. There is no significant difference between the values of F_L and F_D for 10 μm particles. It means that the 10 μm particles sustain their equilibrium position in spite of increase of the total flow rate. However, the 4 μm particles move further to sidewall 2 due to strongly reinforced Dean drag forces.

Even though we can understand the separation mechanism in the CEA microchannel from the estimated theoretical calculations above, there might be some limitations: (1) theoretical assumption of Eq. (4), (2) another inertial fluid phenomenon, vortex by flow separation at expansion regions. It should be noted that the Eq. (4) assumes $Re_p < 1$, which could not cover all the cases of implemented experimental here and might be a source of error in any theoretical predictions. In addition, another inertial fluid phenomenon should be considered for the theoretical analysis in the CEA microchannel at high Re. When the inertial fluid escapes from the contraction region to expansion region, flow separation occurs at the edge of contraction region and induces vortex in the expansion region at the high total flow rate (see the image at a total flow rate of 22 mL/h in Fig. 3). The induced vortex area in the expansion region might play role as a void area, which could result in additional inertial lift forces acting on the particles in the expansion regions. From the computational simulation results, it was observed that the flow velocities between the contraction and expansion region are almost similar due to the void area by vortex in the expansion region (Supporting Information Fig. 1). Not only the change of inertial lift force in the expansion region but also the change of Dean drag force should be considered owing to the change of curved path of the streamlines influenced by the expansion vortex, resulting in the change of the radius of curvature of flowing fluid at the entrance of the contraction region. From these, it is inferred that the Dean drag force is variable according to the size of vortex area in the front expansion region, because the Dean drag force by Dean flow is a function of radius of curvature of the flowing fluid [26].

3.3. Separation of microparticles

Inertial separation of the mixture of 4-μm (red) and 10-μm (green) fluorescent particles was experimentally demonstrated in the CEA microchannel varying the total flow rate from 3 to 22 mL/h (Fig. 3). In order to position the microparticles near to sidewall 1 of the channel, the mixture of microparticles was introduced

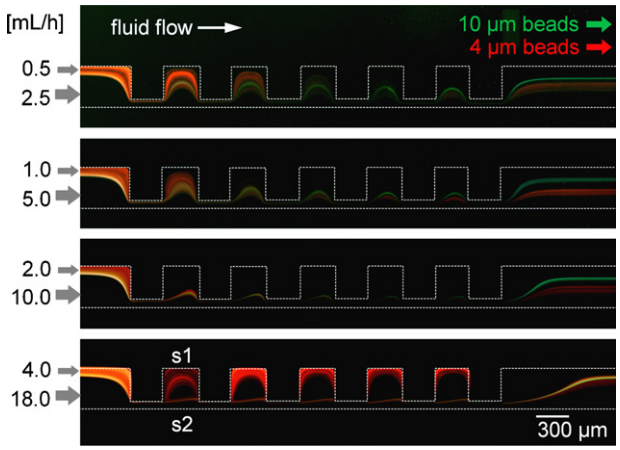

Fig. 3. Fluorescence micrograph images of inertial separation of the mixture of 4-μm (red) and 10-μm (green) fluorescent particles varying the total flow rate (the sum of particle flow rate and focusing flow rate) from 3 to 22 mL/h. (For interpretation of the references to color in this figure legend, the reader is referred to the web version of the article.)

with a focusing flow and then pushed close to sidewall 1. At the first observation window area after passing through six contraction regions, it was observed that the 10 μm particles occupied their equilibrium position near to sidewall 1 by dominated inertial lift forces, while the 4 μm particles migrated toward sidewall 2 by Dean flows. Over the wide range of the total flow rate from 3 to 12 mL/h, the injected two particles were successfully separated from each other after passing the sixth contraction region. However, the two particles could not be separated after passing through the twelfth and eighteenth contraction region, because the 4 μm particles were influenced by Dean flows and continuously followed rotational fluid movements of Dean vortices. Therefore, the particle streams formed a broad band across the channel after passing the twelfth and eighteenth contraction region (Supporting Information Fig. 2).

Inertial separation of the mixture of 10-μm (green) and 15-μm (red) particles was also experimentally performed in the CEA microchannel varying the total flow rate from 3 to 22 mL/h (Fig. 4). Since the F_L and F_D depend on the particle size from the Eqs. (2) and (4), the F_L increases more rapidly than F_D as particle size increases ($F_L \propto a_p^4$ while $F_D \propto a_p$). From this relationship, it is natural that 15 μm particles are dominantly influenced by inertial lift forces

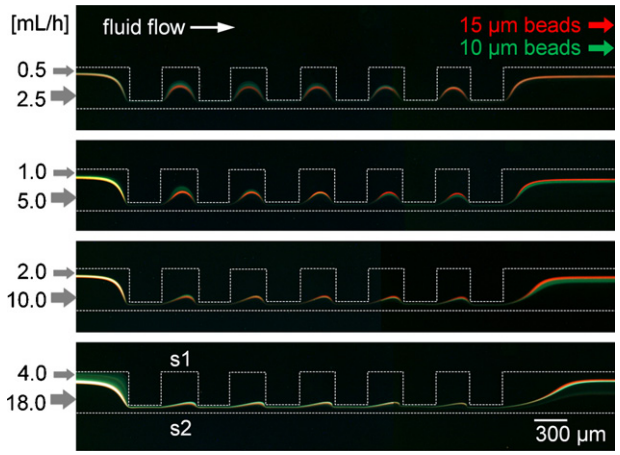

Fig. 4. Fluorescence micrograph images of inertial separation of the mixture of 10-μm (green) and 15-μm (red) fluorescent particles varying the total flow rate of 3–22 mL/h. (For interpretation of the references to color in this figure legend, the reader is referred to the web version of the article.)

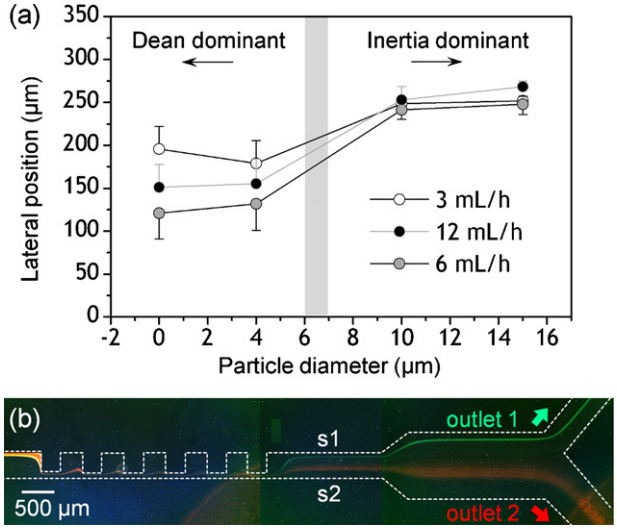

Fig. 5. Separation of microparticles in the bifurcation outlet. (a) Lateral position *versus* fluorescent solution and particle diameter of 4, 10 and 15 μm varying the total flow rate of 3–12 mL/h. (b) Fluorescence micrograph image of inertial separation of 10-μm (green) and 4-μm (red) particles at a total flow rate of 14.5 mL/h. (For interpretation of the references to color in this figure legend, the reader is referred to the web version of the article.)

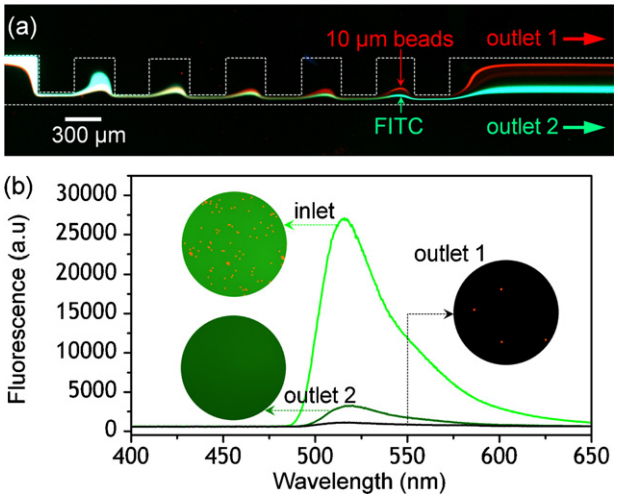

Fig. 6. Exchange of the carrier medium. (a) Fluorescence micrograph image of exchange of the carrier medium while retaining 10 μm beads at a total flow rate of 13 mL/h. (b) Plot of fluorescent intensities at different wavelengths varying from 400 to 650 nm. The emission wavelength of fluorescent solution is approximately 520 nm. The inset images show fluorescent micrographs of the solutions from inlet, outlet 1 and outlet 2. (For interpretation of the references to color in this sentence, the reader is referred to the web version of the article.).

as well as 10 μm particles. For 10 and 15 μm particles, the Dean drag forces barely play role for migration because the two particles occupy a similar equilibrium position under the dominant inertial lift forces. Hereby, the separation is not effective with relatively 10 and 15 μm particles, compared with 4 and 10 μm particles. Even though the injected 10 and 15 μm particles are scarcely separated using a balancing between inertial lift force and Dean drag force, they occupy slightly different equilibrium positions depending on the particle size and the total flow rate from the Eq. (4) ($F_L \propto U_m$ and $F_L \propto a_p^4$). At the whole range of the total flow rate, the injected two particles were observed to sustain their equilibrium position after passing through not only the sixth contraction region, but also the twelfth and eighteenth contraction region (Supporting Information Fig. 3).

In the CEA microchannel, it could be considered for inertial size separation by a specific value of the critical particle size when a large particle above that value is dominated by inertial lift forces; and a small particle below that value is dominated by Dean drag forces. From the experimental results of lateral positions of the particles, we can presume the critical value of 6–7 μm particle size in the CEA microchannel (Fig. 5a). Under the critical value of the particle size, the particles migrate toward sidewall 2 due to the dominated Dean drag forces, while above the critical value of the particles size, the particles occupy their equilibrium positions near to sidewall 1 due to the dominated inertial lift forces. The injected particles are not vertically focused, but only horizontally focused toward sidewall 1 by the focusing flow. The small particles (below than 4 μm) vertically located near to the channel center migrate toward sidewall 2, while the one near to channel top and bottom are firstly pushed into the channel center and migrate to the sidewall 2 afterword due to the dominance of Dean flow. On the other hand, the large particles (more than 10 μm) occupy equilibrium position regardless of the vertical location of the particles due to the dominance of inertial lift force. It causes large and small deviations of experimental results corresponding to small and large particles, respectively.

In order to evaluate the separation efficiency, we designed another CEA microchannel with the bifurcation outlets for collecting particles after the sixth contraction region (corresponding channel length is 3.3 mm) and channel height of 36 μm (Fig. 5b). For inertial separation of microparticles, we introduced a mixture of 4 μm (red) and 10 μm (green) particles into the upper inlet channel at a flow rate of 1 mL/h; and a focusing flow into the bottom inlet channel at a flow rate of 13.5 mL/h. The separation purity was calculated with collected particles at each outlet. The purities are enhanced from 11% to 100% for 10 μm particles and from 89% to 99% for 4 μm particles. The separation throughput was 111 particles/s calculated based on the flow rate of the upper inlet.

3.4. Exchange of the carrier medium

For exchange of the carrier medium, we used a mixture of 10 μm particles (red) and fluorescent solution (green). The mixture was introduced with a focusing flow at a total flow rate of 13 mL/h in the CEA microfluidic device with the bifurcation outlets after the sixth contraction region (Fig. 6a). The inertial lift forces drove the microparticles toward sidewall 1 and the Dean drag forces entrained the fluorescent solution to sidewall 2. Thereby, the microparticles and fluorescent solution began to migrate in opposite directions across the channel and finally separated via the bifurcation. Consequently, the microparticles and fluorescent solution reached at outlet 1 and outlet 2, respectively. In order to verify the efficiency of media exchange, the solutions from inlet, outlets 1 and 2 were inspected by using a spectrometer. The emission wavelength at 520 nm corresponding to emission wavelength of fluorescent solution was scarcely detected with the collected solutions from outlet 1, compared with the injected solution (Fig. 6b). As can be seen at the image from outlet 1, we can acquire pure 10 μm particles where the fluorescent solution was completely eliminated. From these results, it suggests that the CEA microfluidic device can be used for biochemical applications such as rapid treatment and exchange of reagents in a microchannel.

4. Conclusion

We have designed the CEA microchannel enabling inertial size separation of microparticles and fluorescent solution using the force balance between inertial lift and the Dean drag forces. The inertial separation mechanism was theoretically and exper-

imentally demonstrated with numerical simulation results and inertial separation of different-sized particles. The CEA microchannel allows the larger particles (more than 10 μm) to migrate toward sidewall 1 by dominant inertial lift forces and the smaller particles (less than 4 μm) to move away from sidewall 1 by Dean drag forces. The direction of the particle migration is dependent on not only the particles size, but also the total flow rate. Even though the mechanism of inertial separation in the CEA microchannel was described using theoretical analysis, additional inertial effects on the separation should be further considered and discussed such as vortex by flow separation in the expansion regions at high flow rate. In addition, the inertial particle migration might also be considered with viscoelasticity of fluids. For viscoelastic fluids, the particles migrate toward channel center in a cross-section of the channel due to the imbalance in the first normal stress difference between center and the channel wall [27,28]. It can be utilized to modulate the inertial lift force with viscoelastic fluids in order to enhance the inertial particle separation. The proposed channel design for inertial separation allows straightforward, passive, continuous operation and easy integration with other microfluidic components. We expect that this design will allow a wide range of applications in a biochemical, clinical, and environmental field with high-throughput, low-cost and continuous separation.

Acknowledgments

This research was supported by the National Research Laboratory (NRL) Program grant (R0A-2008-000-20109-0) and by the Converging Research Center Program grant (2009-0093663) through the National Research Foundation of Korea funded by the Ministry of Education, Science and Technology (MEST).

Appendix A. Supplementary data

Supplementary data associated with this article can be found, in the online version, at doi:10.1016/j.chroma.2010.11.081.

References

[1] N. Pamme, Lab Chip 7 (2007) 1644.
[2] M. Toner, D. Irimia, Annu. Rev. Biomed. Eng. 7 (2005) 77.
[3] S. Choi, S. Song, C. Choi, J.-K. Park, Lab Chip 7 (2007) 1532.
[4] N. Pamme, A. Manz, Anal. Chem. 76 (2004) 7250.
[5] X.B. Wang, J. Vykoukal, F.F. Becker, Biophys. J. 74 (1998) 2689.
[6] S. Choi, J.-K. Park, Lab Chip 5 (2005) 1161.
[7] M.P. MacDonald, G.C. Spalding, K. Dholakia, Nature 426 (2003) 421.
[8] F. Petersson, A. Nilsson, C. Holm, H. Jonsson, T. Laurell, Lab Chip 5 (2005) 20.
[9] B.P. Ho, L.G. Leal, J. Fluid Mech. 65 (1974) 365.
[10] G. Segre, A. Silberberg, J. Fluid Mech. 14 (1962) 136.
[11] B.G. Segre, A. Silberberg, Nature 189 (1961) 209.
[12] B. Chun, A.J.C. Ladd, Phys. Fluids 18 (2006) 031704.
[13] A.A.S. Bhagat, S.S. Kuntaegowdanahalli, I. Papautsky, Phys. Fluids 20 (2008) 101702.
[14] D. Di Carlo, D. Irimia, R.G. Tompkins, M. Toner, Proc. Natl. Acad. Sci. U.S.A. 48 (2007) 18892.
[15] I. Gregoratto, C.J. McNeil, M.W. Reeks, Proc. SPIE 6465 (2007) 646503.
[16] J. Seo, M.H. Lean, A. Kole, J. Chromatogr. A 1162 (2007) 126.
[17] A.A.S. Bhagat, S.S. Kuntaegowdanahalli, I. Papautsky, Lab Chip 8 (2008) 1906.
[18] M.G. Lee, S. Choi, J.-K. Park, Appl. Phys. Lett. 95 (2009) 051902.
[19] M.G. Lee, S. Choi, J.-K. Park, Lab Chip 9 (2009) 3155.
[20] M.G. Lee, S. Choi, J.-K. Park, Biomed. Microdevices 12 (2010) 1019.
[21] S. Choi, S. Song, C. Choi, J.-K. Park, Anal. Chem. 81 (2009) 50.
[22] J.-P. Matas, J. Morris, E. Guazzelli, Oil Gas Sci. Technol. 59 (2004) 59.
[23] J.-P. Matas, J. Morris, E. Guazzelli, J. Fluid Mech. 515 (2004) 171.
[24] E.S. Asmolov, J. Fluid Mech. 381 (1999) 63.
[25] D. Di Carlo, J.F. Edd, D. Irimia, R.G. Tompkins, M. Toner, Anal. Chem. 80 (2008) 2204.
[26] S.A. Berger, L. Talbot, Annu. Rev. Fluid Mech. 15 (1983) 461.
[27] B.P. Ho, L.G. Leal, J. Fluid Mech. 76 (1976) 783.
[28] S. Yang, J.Y. Kim, S.J. Lee, S.S. Lee, J.M. Kim, Lab Chip 11 (2011) 266.